Int. J. Electrochem. Sci., 13 **(2018)** 1147 – 1160, doi: 10.20964/2018.01.70

International Journal of
ELECTROCHEMICAL
SCIENCE
www.electrochemsci.org

Porous Core-Shell SnO_2 fibers/rGO Composite and Its Lithium Storage Performance

Ji Yu [1], *Li Li*[1], *Zishuang Yue* [1], *Zhenyu Yang*[1], *Jianxin Cai*[2,*]

[1] Department of Chemistry, Nanchang University, No. 999 Xuefu Road, Nanchang 330031, P. R. China
[2] School of Resources Environmental and Chemical Engineering, Nanchang University, No. 999 Xuefu Road, Nanchang 330031, P. R. China
[*]E-mail: cjx@ncu.edu.cn

Received: 12 October 2017 / *Accepted:* 8 November 2017 / *Published:* 16 December 2017

In this work, a porous core–shell composite composed of reduced graphene oxide (rGO)-wrapped SnO_2 fibers (SnO_2 fibers/rGO composite) was fabricated through electrospinning assisted by pyrolysis. The special core–shell structure showed that porous SnO_2 fibers as the "core" were completely protected by multilayer rGO as the "shell." Lithiation of SnO_2 occurred through Li diffusion through the rGO wrapped into the SnO_2 fibers, and natural void space facilitated SnO_2 expansion upon lithiation. This unique structure effectively prevented the aggregation and pulverization of SnO_2 fibers during lithiation and delithiation. The SnO_2 fibers/rGO composite electrode presented a super-high discharge capacity of 2,141 mAh g^{-1} at a current density of 0.4 A g^{-1}, 1,858 mAh g^{-1} at 0.8 A g^{-1}, 1,520 mAh g^{-1} at 1.6 A g^{-1}, and 874 mAh g^{-1} at 2.0 A g^{-1} after 10 cycles. The electrode showed a discharge capacity of 658 mAh g^{-1} at a current density of 4 A g^{-1} after 1,000 cycles.

Keywords: porous, core–shell, tin oxide fibers, rGO, Li storage performance

1. INTRODUCTION

Lithium-ion batteries (LIBs) are advanced energy storage devices that have penetrated markets for portable electronic devices and new energy automobile, such as mobile phones, laptops, and hybrid electric vehicles [1–3]. The increased usage of such batteries is attributed to their superior electrochemistry properties, including high energy density, long cycle life, and good power performance [4, 5]. However, the anode materials in commercial LIBs are mainly based on graphite or other carbon materials with a low capacity of 372 mAh g^{-1} and thus cannot meet the continuously increasing demand for high-performance LIBs [5–8].

Tin oxide (SnO_2) is one of the ideal anode material candidates for next-generation LIBs due to its high capacity, low cost, abundance, and low toxicity [7, 9, 10]. However, the practical application of SnO_2 is limited by large volume change (~300%) and agglomeration during lithiation and delithiation, and these occurrences result in a limited cycle life [11–14]. Various SnO_2 nanostructures, such as nanotubes [15, 16], fibers [3, 5, 9, 17], hollow spheres [18–20], and nano boxes [9, 21], have been studied to overcome these shortcomings. SnO_2-based composites, such as SnO_2/C, are good anode materials with long cycle life because of the effects of cushioning and good electrical conductivity [22, 23]. Several recent studies have shown that SnO_2 fibers supported by carbon matrices exhibit improved Li storage performance because of their unique structural and compositional features [24–27]. Further exploration and rational fabrication of SnO_2 composite electrode materials with high-rate performance and long cycle life will significantly affect the practical utilization of such materials in LIBs.

In this work, we fabricated a novel core–shell structure composed of SnO_2 fibers/reduced graphene oxide (rGO) anode materials via electrostatic self-assembly. Positively charged SnO_2 fibers were wrapped with negatively charged graphene layers in the preparation process. As shown in Figure 1, the porous SnO_2 fibers were considered the "core," and the wrapped multilayer rGO served as the "shell." This unique core–shell structure presents several advantages for Li storage. First, the void space between the SnO_2 fibers and rGO layers allows SnO_2 to expand upon lithiation. Second, the rGO layers prevent the electrolyte from completely reaching the SnO_2 surface inside the rGO layers, and lithiation of SnO_2 occurs through Li diffusion through rGO into the SnO_2 fibers. Third, the rGO layers are electronically and ionically conducting, which results in good kinetics in the SnO_2 fibers/rGO anode. The SnO_2 fibers/rGO composite electrode demonstrated a remarkable Li-storage performance.

2. EXPERIMENTAL

2.1. Materials

Poly(vinyl pyrrolidone) (PVP, Mw = 1,300, 000) and $SnCl_2{\cdot}2H_2O$ were obtained from Aladdin. N, N-dimethylformamide (DMF, AR) was purchased from Sinopharm Chemical Reagent Co., Ltd. These reagents were used without further purification.

2.2. Preparation of SnO_2 fibers

Approximately 4.42 g of DMF was dissolved in ethanol, and 2 wt.%, 5 wt.%, and 8 wt.% (vs. DMF ethanol solution) $SnCl_2{\cdot}2H_2O$ powder was added to the solution and stirred vigorously at room temperature for 4 h. Afterward, 4.36 g of PVP ethanol solution was added and stirred for another 3 h to obtain the precursor solution.

The SnO_2 fibers were prepared by electrospinning. The precursor solution was placed in a plastic syringe equipped with a stainless steel needle with a diameter of 0.8 mm and electrospun at a DC voltage of 10 kV. The flow rate was 0.5 mL h^{-1}. PVP/as-SnO_2 fibers were collected on aluminum

foil, which was placed 15 cm under the needle. The fibers were placed in a vacuum oven for 12 h at room temperature to remove the residual solvent and calcined at 500 °C for 3 h in air to obtain SnO_2 fibers. The heating rate was 5 °C min^{-1}. The as-prepared samples were labeled as 2%-SnO_2 fibers, 5%-SnO_2 fibers, and 8%-SnO_2 fibers.

2.3. Preparation of GO

GO was synthesized from natural graphite through a modified Hummers method [28, 29]. A total of 50 mL of concentrated H_2SO_4 was added to a mixture composed of 2 g of graphite and 1 g of $NaNO_3$ powder in a flask maintained at 5 °C and stirred for 30 min. Then, 7 g of $KMnO_4$ was added to the solution in four portions within 90 min. The temperature of the solution was increased to 35 °C afterward and maintained for 4 h. Then, 90 mL of deionized water and 7 mL of 30% H_2O_2 were added. The depositions were collected and washed with 150 mL of 3% HCl solution. The precipitate was dispersed in 800 mL of deionized water, re-collected by centrifugation, and placed in a dialysis bag for 7 d.

2.4. Fabrication of the SnO_2 fibers/rGO composite

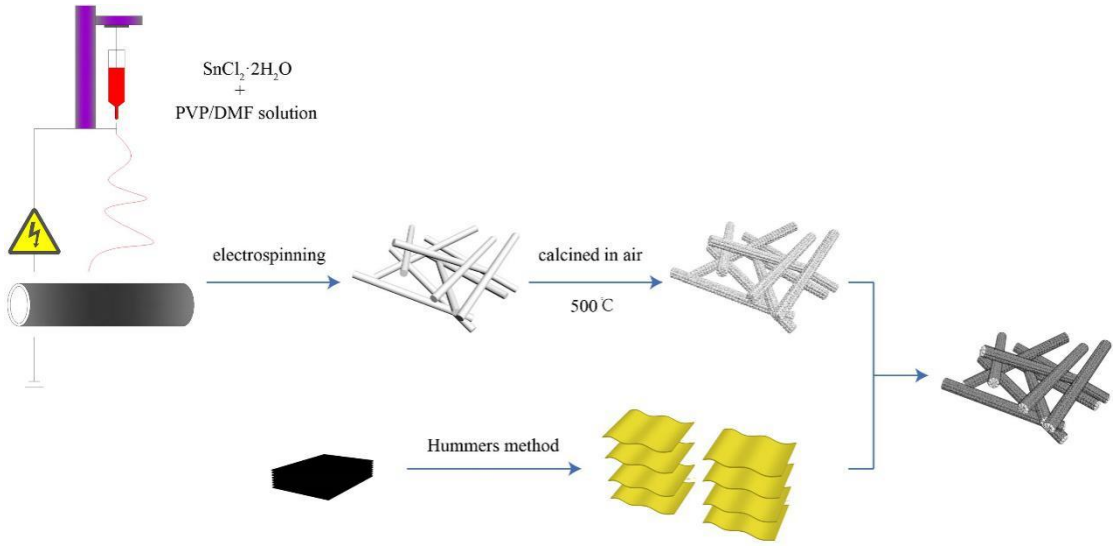

Figure 1. Schematic of the fabrication of the SnO_2 fibers/rGO composite

A homogeneous suspension of GO and SnO_2 fibers was carefully prepared to create the SnO_2 fibers/rGO composite. Approximately 200 mL of alcoholic GO (1.15 mg ml^{-1}) was sonicated for 30 min to form a stable solution. Subsequently, SnO_2 fibers of a certain quality were mixed with alcoholic GO (15 mL) and sonicated for another 30 min to form a homogeneous dispersion. The SnO_2 fibers/GO composite was collected by centrifugalization after 2 d. The collected powders were dried at 60 °C in a vacuum and calcined at 300 °C for 1 h under the protection of argon to obtain the final SnO_2 fibers/rGO composite. Notably, the color of the final product changed from bright white to dark white after calcination. 2%-SnO_2 fibers/rGO, 5%-SnO_2 fibers/rGO, and 8%-SnO_2 fibers/rGO composites

were prepared under similar conditions for the comparison of electrochemical performance. The fabrication of the SnO_2 fibers/rGO composite is illustrated in Figure 1.

2.5. Characterization

The morphology of the samples was characterized with a scanning electron microscope (SEM, FEI Quanta200F) and a transmission electron microscope (TEM, FEI Tecnai G2 F20, 200 kV). The crystalline structure of the samples was characterized through X-ray diffraction (XRD) using a diffractometer (Bruker D8 Focus X-ray diffractometer), and the diffraction patterns were recorded at room temperature in the 2θ range between 5° and 80°. Weight loss behavior was tested in air through thermogravimetric (TG) analysis (TGA/DSC 3+, Mettler Toledo, Zurich, Switzerland). Raman spectra were recorded using a confocal Raman microscope (Renishaw, Invia) at 633 nm excitation. XPS information was collected with Thermo ESCALAB250Xi.

2.6. Electrochemical performance test

The electrochemical properties of the SnO_2 fibers and SnO_2 fibers/rGO composite were investigated by constructing a CR2025 coin half-cell with lithium foil as a counter electrode. The half-cell was assembled in a glove box (Mbraun Lab Master 130, Germany) containing high-purity argon atmosphere. Celgard® 2325 was used as a separator. The electrolyte was composed of 1 M $LiPF_6$ dissolved in a mixture of ethylene carbonate (EC) and dimethyl carbonate (DMC) (1:1 in vol.). The as-prepared samples and a certain amount of C_2H_5OH were mixed to form a slurry to prepare the anodes, and the slurry was attached to the surface of copper foil and dried in a vacuum at 60 °C for 24 h. No conductor and binder were used. Electrochemical impedance spectroscopy (EIS) was performed with an electrochemical workstation (PARSTAT 2273, Prinston, USA) with a frequency range of 10 mHz to 100 kHz. Constant-current charge and discharge tests were conducted with a multi-channel battery test system (NEWARE, China) at different current densities between cutoff potentials of 0.02 and 2.50 V. The charge and discharge capacities were calculated on the basis of the weight of SnO_2 fibers or SnO_2 fibers/rGO composite (0.8 mg cm^{-1} per electrode).

3. RESULTS AND DISCUSSION

The XRD spectrum of the as-prepared SnO_2 fibers is shown in Fig. 2. The main diffraction peaks at 2θ = 26.70°, 33.79°, 33.67°, 51.51°, and 54.24° can be indexed to the planes of (110), (101), (200), (211), and (220) of rutile SnO_2, respectively (JCPDS 41-1445) [17, 19, 30]. This result indicates that SnO_2 fibers were successfully synthesized, and no impurities (e.g., $SnCl_2$ and SnO) existed in the sample.

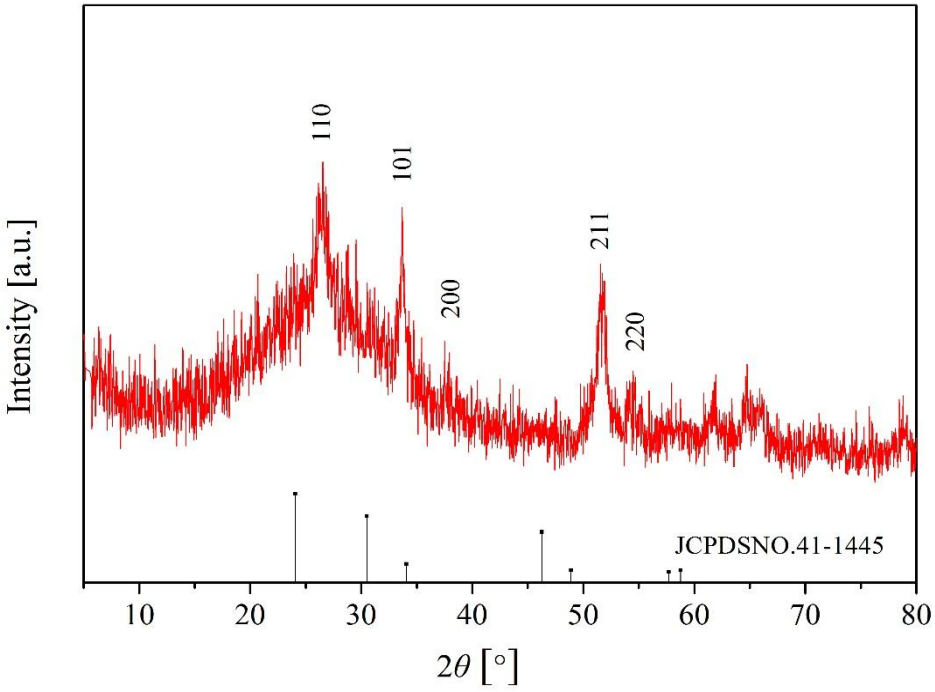

Figure 2. XRD patterns of the SnO_2 fibers with reference to rutile SnO_2

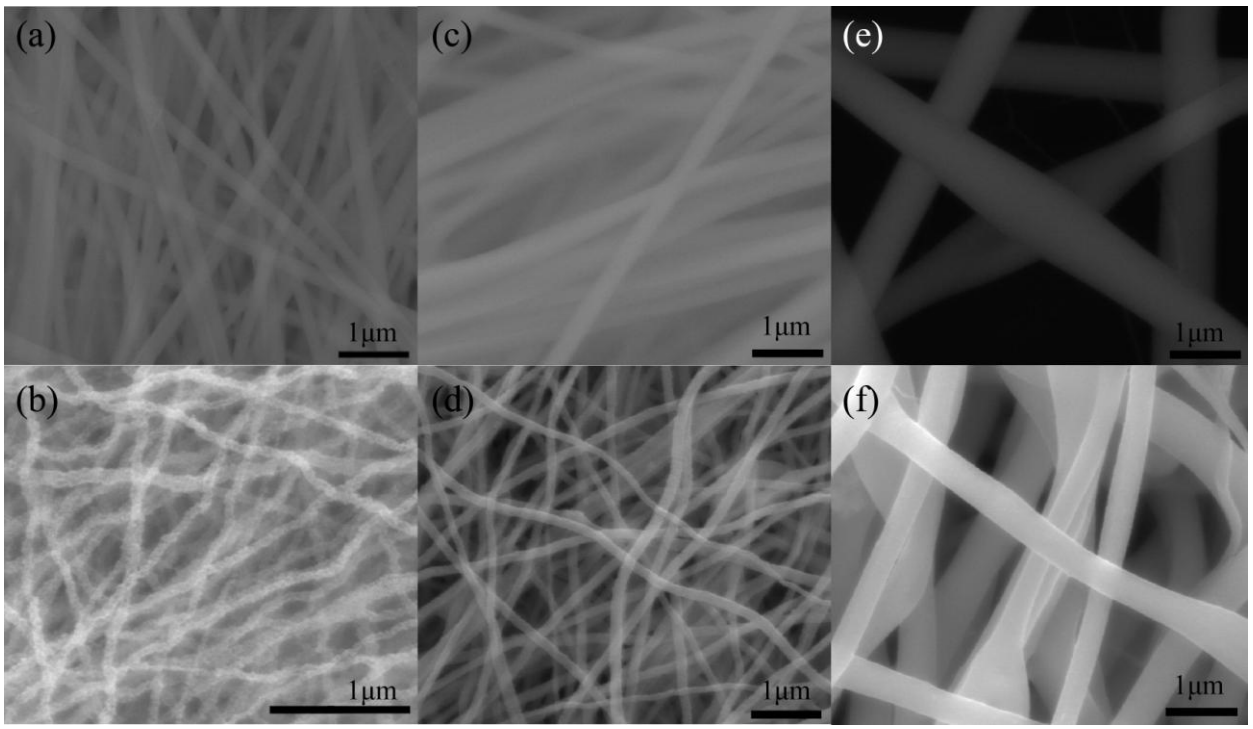

Figure 3. SEM images of (a) 2%-, (c) 5%-, and (e) 8%-PVP/SnO_2 fibers and (b) 2%-, (d) 5%-, and (f) 8%-SnO_2 fibers after calcination in air

The influence of the concentration of $SnCl_2$ in the DMF ethanol solution on the morphology of the SnO_2 fibers was investigated. Three different weight ratios (vs. DMF ethanol solution) of $SnCl_2$

with contents of 2%, 5%, and 8% were applied. Figs. 3(a), 3(c), and 3(e) show the SEM images of 2%, 5%, and 8%-PVP/SnO_2 fibers. Figs. 3(b), 3(d), and 3(f) show the SEM images of 2%, 5%, and 8%-SnO_2 fibers prepared by calcining PVP/as-SnO_2 fibers in air at 500 °C for 3 h. Figs. 3(a), 3(c), and 3(e) show that the diameter of the smooth PVP/SnO_2 fibers increased from ~300 nm to ~400 nm and ~800 nm when the contents of $SnCl_2$ increased from 2 wt.% to 5 wt.% and 8 wt.%. This phenomenon can be explained by the increment in the viscosity of the solution resulting from an increase in the concentration of $SnCl_2$ and the adhesion of the fibers to form bulkier fibers [31]. After heat treatment, the average diameter of the as-obtained SnO_2 fibers shrank to 100, 250, and 500 nm for the sample of 2%, 5%, and 8%-SnO_2 fibers, respectively, and the surface of the SnO_2 fibers became rough and porous due to the decomposition of PVP, as shown in Figs. 3(b), 3(d), and 3(f).

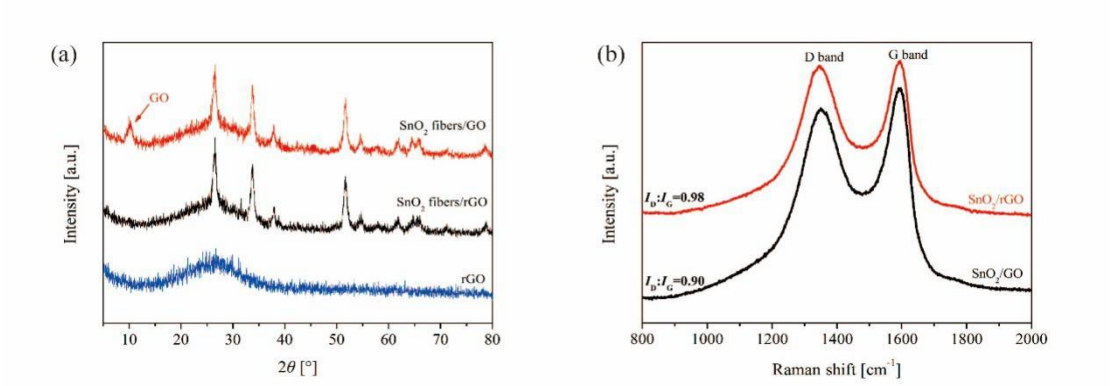

Figure 4. (a) XRD patterns of the 2%-SnO_2 fibers/GO, 2%-SnO_2 fibers/rGO, and rGO samples; (b) Raman spectra of the 2%-SnO_2 fibers/GO and 2%-SnO_2 fibers/rGO samples

Figure 4(a) shows the XRD patterns of the 2%-SnO_2 fibers/GO composite, 2%-SnO_2 fibers/rGO composite, and rGO composite. The samples of 5%- and 8%-SnO_2 fibers/GO or rGO composite showed similar XRD patterns, which are not given in this manuscript. The peak at 2θ=9.88° is a characteristic diffraction peak of GO, which was displayed in the sample 2%-SnO_2 fibers/GO composite and disappeared in the sample 2%-SnO_2 fibers/rGO composite after calcination, indicating the reduction of GO. The rest of the peaks in the XRD patterns of the 2%-SnO_2 fibers/GO or rGO composite can be indexed to rutile SnO_2 (cassiterite, JCPDS No. 41-1445). Notably, the peak at about 26.8° corresponding to the (002) plane of rGO almost overlapped with the (110) peak of rutile SnO_2 [32, 33]. Raman spectroscopy is a useful tool to analyze the disordered carbon. The Raman spectra of the sample 2%-SnO_2 fibers/GO and 2%-SnO_2 fibers/rGO composites are presented in Fig. 4(b). Both samples show two prominent peaks at about 1596 and 1346 cm^{-1}, which correspond to the G and D bands, respectively. The intensity ratio of D to G band (I_D/I_G) is 0.90 and 0.98 for the sample of 2%-SnO_2 fibers/GO and 2%-SnO_2 fibers/rGO composite. The increase in the intensity ratio indicated an increase in material defects after heat treatment, which is in agreement with the fact that heat decomposition of GO increases vacancies on the graphene plane and defects at the boundaries [33, 34].

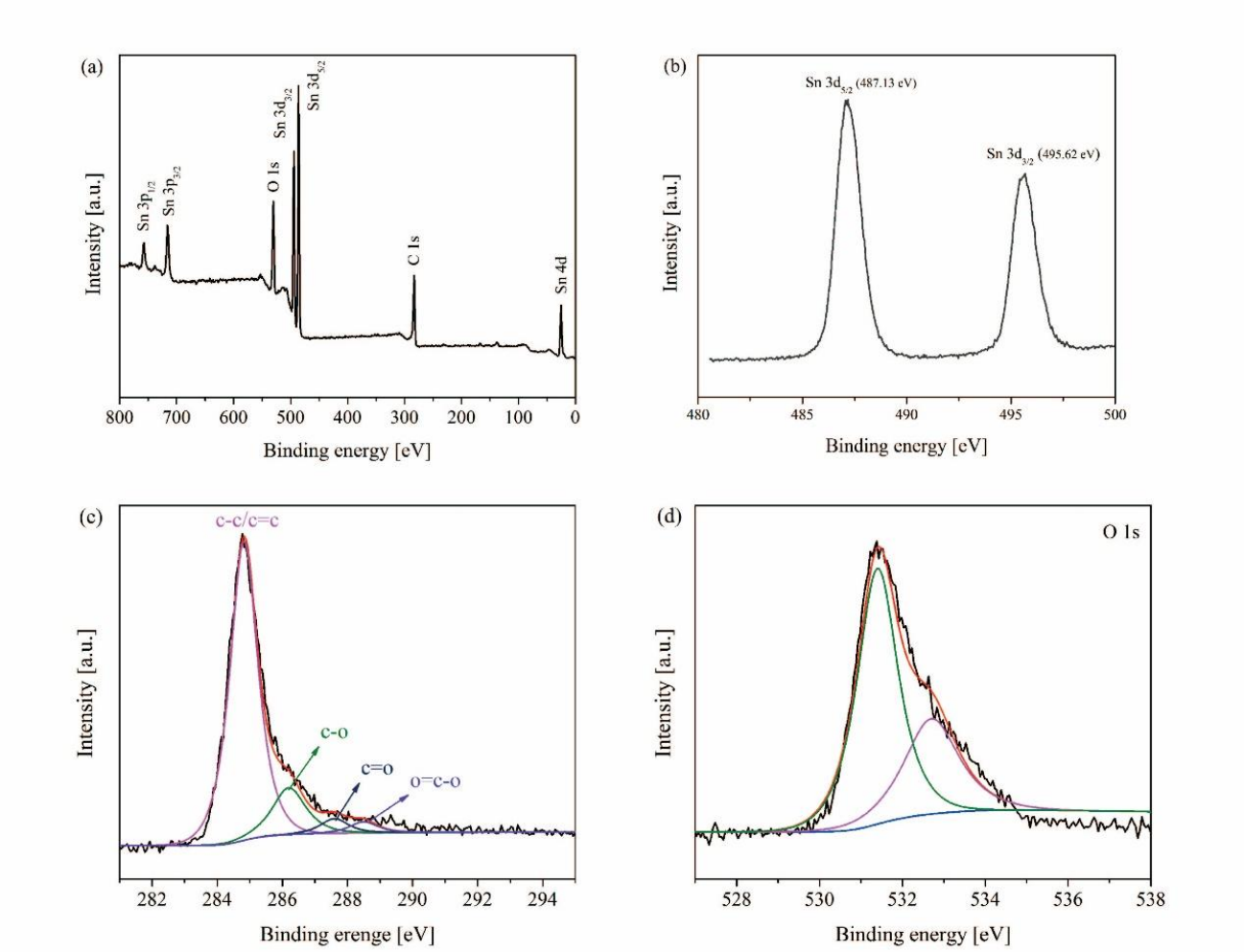

Figure 5. XPS survey spectrum of (a) 2%-SnO_2 fibers/rGO, (b) Sn 3d peak, (c) C1 s peak, and (d) O1s 3d peak

XPS can provide useful information on the elemental composition of compounds and the chemical states of their elements. As shown in Fig. 5(a), the survey scan spectrum only revealed peaks of tin, oxygen, and carbon, indicating the high purity of the as-prepared SnO_2 fibers/rGO composite. Fig. 5(b) shows a high-resolution XPS spectrum of Sn 3d. The two symmetrical peaks at 487.13 and 495.62 eV with a peak separation of 8.49 eV can be ascribed to $3d_{3/2}$ and $3d_{5/2}$ of Sn (IV), respectively, and suggest the existence of Sn^{4+} in the composite [27, 33]. The C 1s peaks (Fig. 5(c)) can be fitted to line shapes with binding energies at 284.8, 286.2, 287.6, and 288.5 eV corresponding to C=C/C-C, C-O, C=O, and O=C-O bonds, respectively [35]. The O 1s peak (Fig. 5(d)) can be deconvoluted into two sub-bands at 531.4 and 532.7 eV. The band at 531.4 eV corresponds to the lattice oxygen in SnO_2 species, and the band at 532.7 eV corresponds to the residual oxygen-containing functional groups of the rGO nano sheets and H_2O molecules adsorbed [25].

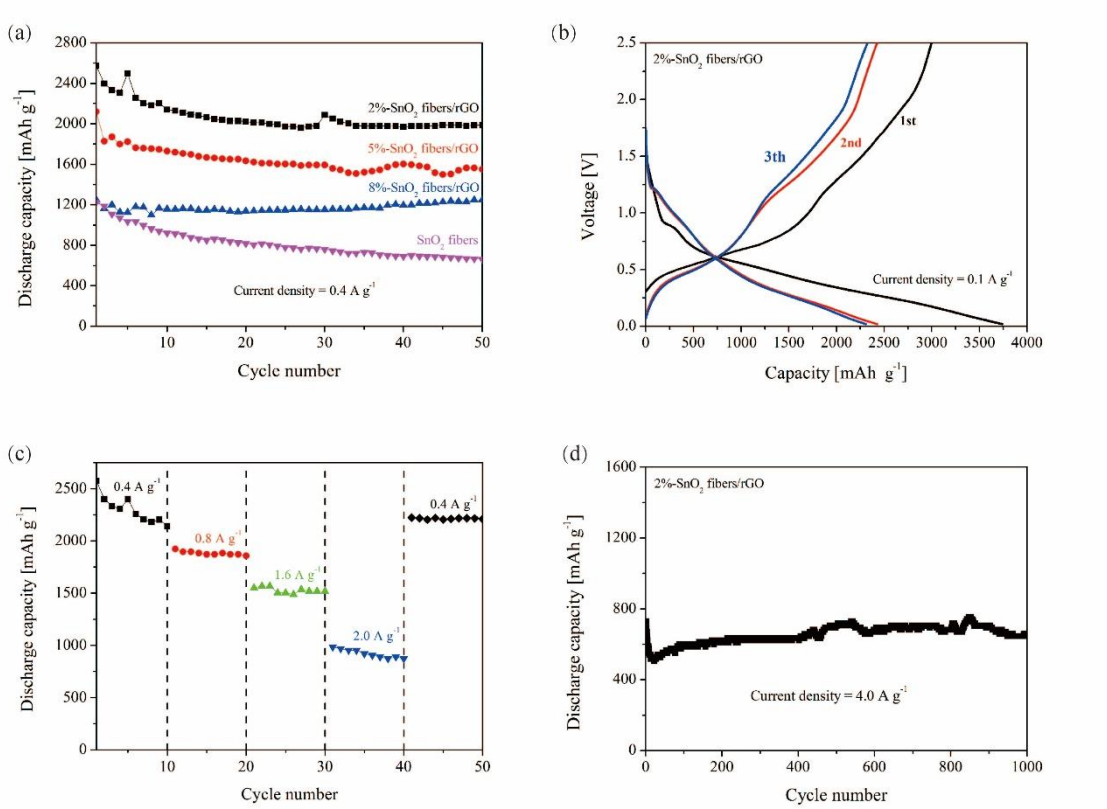

Figure 6. (a) Cycle performance of 2%-, 5%-, and 8%-SnO_2 fibers/rGO composites and SnO_2 fibers at a current density of 0.4 A g^{-1}; (b) galvanostatic lithiation/delithiation curves of the 2%-SnO_2 fibers/rGO composite for the first three cycles at a current density of 0.1 A g^{-1}; (c) rate performance curves of the 2%-SnO_2 fibers/rGO composite; and (d) long cycle performance of the 2%-SnO_2 fibers/rGO composite at a current density of 4 A g^{-1}

To study the electrochemical characteristics of the SnO_2 fibers/rGO composite, the cycle performance of 2%-, 5%-, and 8%-SnO_2 fibers/rGO composites was examined at a current density of 0.4 A g^{-1}. The results are shown in Fig. 6(a). The SnO_2 fibers/rGO composites displayed a better electrochemical performance than bare SnO_2 fibers in all the cases. All three composites showed an excellent cycle performance, but the sample of 2%-SnO_2 fibers/rGO was particularly prominent. After 50 cycles, the 2%-SnO_2 fibers/rGO composite could still present a high discharge capacity of 1,982 mAh g^{-1}, whereas the 5%- and 8%-SnO_2 fibers/rGO composites and bare SnO_2 fibers could only present a discharge capacity of 1,548, 1236, and 668 mAh g^{-1}, respectively. The improved Li-storage performance of the SnO_2 fibers/rGO composites can be attributed to the good electron transfer property of the rGO network and the stability of the electrode [36, 37]. The unique continuous nanofiber structure not only provides a short Li-ion diffusion path but also makes the charge transfer fast because of the continuous electronic channel along the fibers. Moreover, fibers with small diameters can provide a large contact area between the electrode and electrolyte and many active sites for electrochemical reactions [9].

Figure 6(b) shows the first three charge–discharge voltage profiles of the 2%-SnO_2 fibers/rGO composite at a constant current density of 0.1 A g^{-1} within a voltage range of 0.01 V to 2.50 V. The

initial discharge capacity of the composite was approximately 3,740 mAh g^{-1} and then decayed to 2,428 mAh g^{-1} in the second cycle (ICE=65%). Notably, a plateau was observed at 0.88 V in the first cycle but not in the second and third cycles, resulting in a large irreversible discharge capacity loss, which could be caused by the formation of a solid electrolyte interface (SEI) layer on the surface of the electrode and the decomposition of the electrolyte and formed Li_2O [18, 38].

The rate performance of the 2%-SnO_2 fibers/rGO composite at different current densities ranging from 0.4 A g^{-1} to 4.0 A g^{-1} is shown in Figs. 6(c) and 6(d). The discharge capacity of the composite reached 2,141, 1,858, 1,520, and 874 mAh g^{-1} at current densities of 0.4, 0.8, 1.6, and 2.0 A g^{-1}, respectively, after 10 cycles. When the current density decreased to 0.4 A g^{-1}, a significantly high discharge capacity of 2,112 mAh g^{-1} was recovered, showing the excellent rate performance and capability for restoration of the composite. Furthermore, the composite had a long life as shown in Fig. 6(d). The composite could still present a high reversible discharge capacity of 658 mAh g^{-1} at a current density of 4 A g^{-1} after 1,000 cycles. Almost all of the electrochemical properties of this porous core–shell SnO_2 fibers/rGO composite, such as highest discharge capacity, cycling performance, and rate performance, are the best among all the properties of available composites in published literature (Table 1).

Table 1. Comparison of the electrochemical performance of different SnO_2 anodes reported in literature and that in this work

Products	Highest discharge capacity	Cycling performance	Rate performance	Ref.
3D h-SnO_2-Fe_2O_3@rGO	2150 mAh g^{-1} at 200 mA g^{-1}	830 mAh g^{-1} at 200 mA g^{-1} after 100 cycles	550 mAh g^{-1} at 1000 mA g^{-1}	1
Amorphous-SnO_2 /graphene aerogel	1380 mAh g^{-1} at 100 mA g^{-1}	700 mAh g^{-1} at 100 mA g^{-1} after 80 cycles	269 mAh g^{-1} at 1600 mA g^{-1}	2
C/SnO_2/C nanofibers	1050 mAh g^{-1} at 52 mA g^{-1}	837 mAh g^{-1} at 52 mA g^{-1} after 200 cycles	180 mAh g^{-1} at 5220 mA g^{-1}	3
Graphene Encapsulated SnO_2	1802 mAh g^{-1} at 158 mA g^{-1}	682 mAh g^{-1} at 158 mA g^{-1} after 30 cycles	237 mAh g^{-1} at 1580 mA g^{-1}	20
RGO/SnO_2/polyaniline	1560 mAh g^{-1} at 200 mA g^{-1}	1280 mAh g^{-1} at 200 mA g^{-1} after 200 cycles	397 mAh g^{-1} at 10000 mA g^{-1}	33
SnO_2@rGO	1710 mAh g^{-1} at 100 mA g^{-1}	553 mAh g^{-1} at 500 mA g^{-1} after 100 cycles	240 mAh g^{-1} at 1600 mA g^{-1}	34
Nano-walls of SnO_2/rGO	998 mAh g^{-1} at 100 mA g^{-1}	855 mAh g^{-1} at 100 mA g^{-1} after 100 cycles	460 mAh g^{-1} at 1000 mA g^{-1}	35
Porous carbon networks containing Si and SnO_2	2300 mAh g^{-1} at 500 mA g^{-1}	1359 mAh g^{-1} at 500 mA g^{-1} after 200 cycles	512 mAh g^{-1} at 20000 mA g^{-1}	38
Porous core–shell SnO_2 fibers/rGO	3740 mAh g^{-1} at 100 mA g^{-1}	658 mAh g^{-1} at 4000 mA g^{-1} after 1000 cycles	752 mAh g^{-1} at 4000 mA g^{-1}	This work

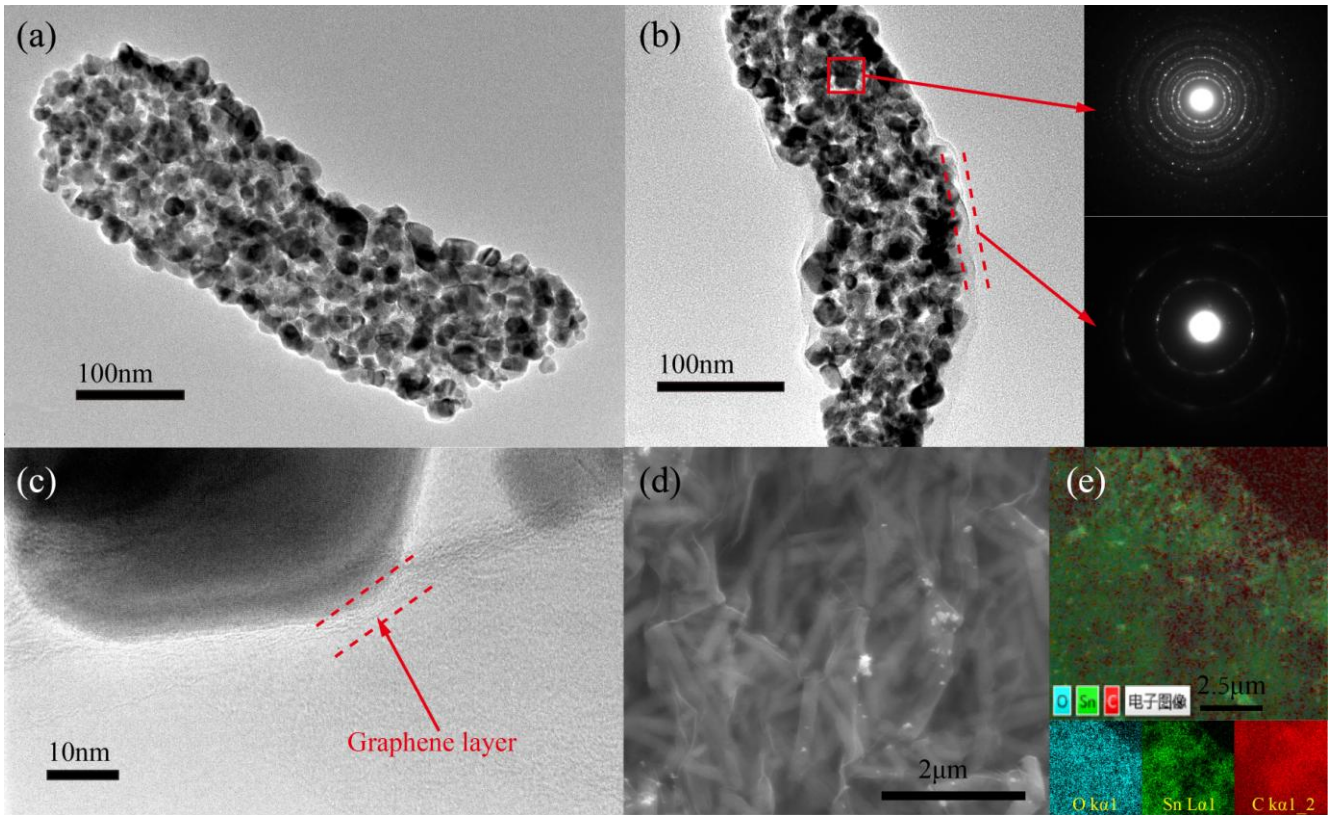

Figure 7. (a) TEM image of 2%-SnO_2 fibers; (b) TEM and SAED images of the 2%-SnO_2 fibers/rGO composite; (c) HRTEM image of the 2%-SnO_2 fibers/rGO composite; (d) SEM image of the 2%-SnO_2 fibers/rGO composite; and (e) elemental mapping with the relative intensities of C (red), Sn (green), and O (blue) of the 2%-SnO_2 fibers/rGO composite

The composite possesses a special structure that can not only withstand long cycling, but is also favorable for rapid electrochemical reactions. As can be seen in the TEM image of 2%-SnO_2 fibers in Fig. 7(a), the fibers have a porous structure because of the decomposition of PVP in the process of heat treatment. The average diameter of the pores is about 5 nm to 10 nm. Figure 7(b) presents the TEM image and selected-area electron diffraction (SAED) patterns of the 2%-SnO_2 fibers/rGO composite. The SAED patterns in Fig. 7(b) can be indexed to SnO_2 and rGO, respectively, which means the SnO_2 fibers were coated by rGO. The SnO_2 fibers wrapped by graphene helped relieve the strain induced by the volume change in the charge–discharge process. The rGO worked as a good barrier to prevent the SnO_2 fibers from aggregating and provided a good conductive network for the anode. In addition, the high-resolution TEM image of the 2%-SnO_2 fibers/rGO composite shows the existence of rGO (Fig. 7(c)). The SEM image and elemental mapping of the 2%-SnO_2 fibers/rGO composite are shown in Figs. 7(d) and 7(e). The SnO_2 fibers shortened after the sonicated treatment and were covered with rGO films, which made the composite appear smooth and shiny. The elemental mapping in Fig. 7(e) shows that the C, O, and Sn elements were distributed throughout the SnO_2 fibers/rGO composite. Usually, many oxygen-containing functional groups (hydroxyl, carbonyl, and carboxyl groups) exist on the surface of GO and act as anchor sites and interact strongly with the covered species [32, 36]. When the solution of negatively charged GO and positively charged SnO_2 fibers was mixed in this

study, the SnO_2 fibers were absorbed easily on the surface of GO due to electrostatic self-assembling interaction.

The thermal gravity of the 2%-SnO_2 fibers/rGO composite was investigated by TG measurement, as shown in Fig. 8. The 2%-SnO_2 fibers/rGO composite was heated in air form 25 °C to 800 °C. The weight loss under 200 °C corresponds to the loss of moisture and the trapped solvent. The weight loss between 200 °C and 600 °C can be attributed to the decomposition of rGO in the composite. No further weight loss was observed above 600 °C. According to the data, the content of SnO_2 in the SnO_2 fibers/rGO composite was 76.3%. In other words, the mass of SnO_2 fibers in the composite accounted for the majority. Notably, the charge–discharge capacity of the cell was calculated based on the quality of the SnO_2 fibers/rGO composite rather than the quality of the SnO_2 fibers.

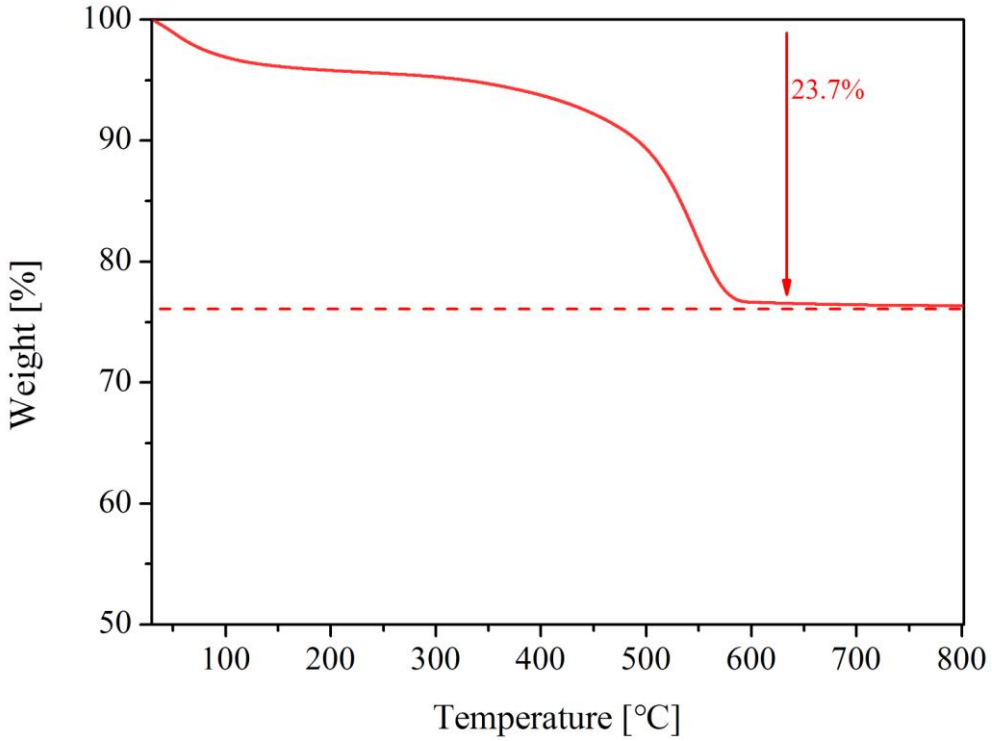

Figure 8. TG curve of the 2%-SnO_2 fibers/rGO composite heated in air from 25 °C to 800 °C at a rate of 10 °C min^{-1}

To understand the electrochemical impedance of the different samples, EIS measurements were carried out on a fresh cell with 2%-, 5%-, and 8%-SnO_2 fibers/rGO composite electrodes. The results are shown in Fig. 9, and the equivalent circuit is shown in the inset. In the equivalent circuit, R_Ω, R_l, R_{ct}, Z_w, and and *CPE* correspond to electrolyte resistance, SEI resistance, charge-transfer resistance, Warburg impedance associated with the diffusion of Li^+, and constant phase element related to double layer capacitance, respectively [39, 40]. The fitting results are shown in Table 2. With a decrease in the content of $SnCl_2$ in the DMF/PVP ethanol solution, R_{ct} decreased, which meant the diffusion of the Li^+

ion from the electrolyte to electrode became easy. This result can be explained by the fact that a sample synthesized at low concentrations has numerous pore structures. This sample has a large contact area with the electrolyte, thus making the reaction easy and fast. The space in the pores can cushion the large volume change during the charge–discharge process for the electrode to provide enhanced electrochemical performance, such as increased cycle life.

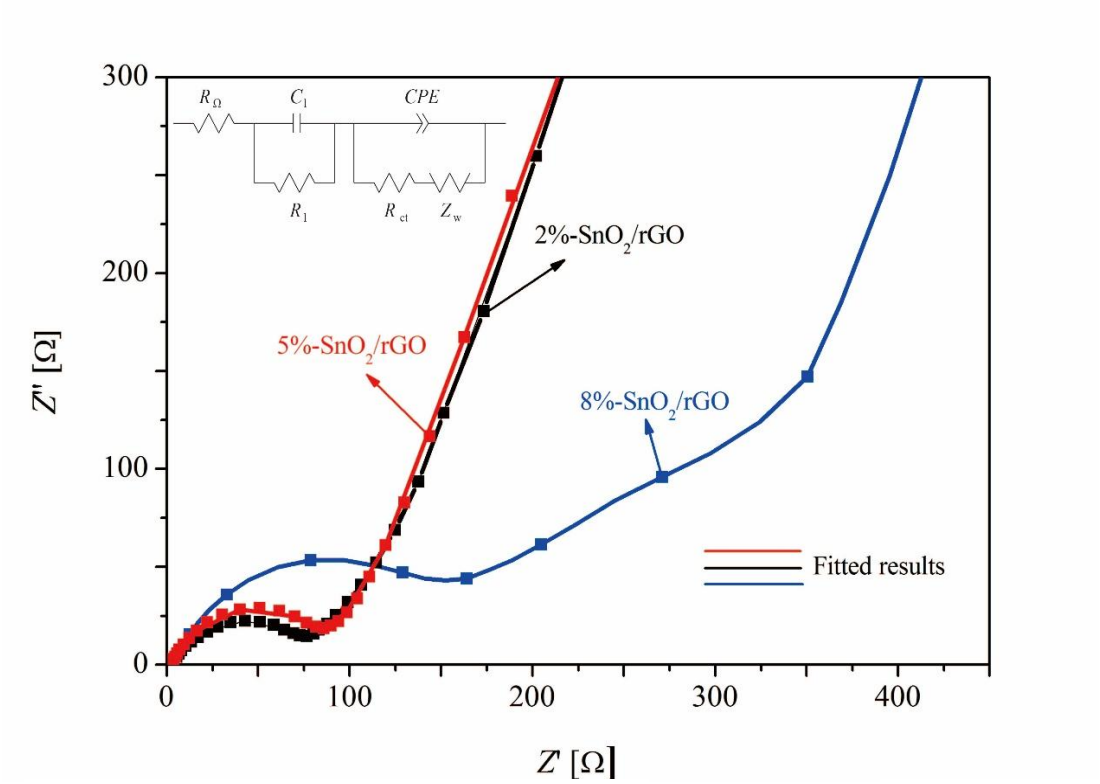

Figure 9. EIS plots of the 2%-, 5%-, and 8%-SnO_2 fibers/rGO composites in the frequency range of 1000 kHz to 10 mHz; the inset is the equivalent circuit

Table 2. Equivalent circuit parameters of the 2%-, 5%-, and 8%-SnO_2 fibers/rGO composite electrodes

Samples	$R_\Omega(\Omega cm^2)$	$R_1(\Omega cm^2)$	*R*ct
2%-SnO_2 fibers/rGO composite	2.141	0.78	83.84
5%-SnO_2 fibers/rGO composite	2.366	0.122	87.63
8%-SnO_2 fibers/rGO composite	3.963	0.892	139.7

4. CONCLUSION

Porous core–shell composites of SnO_2 fibers/rGO were fabricated through electrospinning assisted by pyrolysis. The special core–shell structure revealed that porous SnO_2 fibers as the "core" were completely protected by multilayer rGO as the "shell." Lithiation of SnO_2 occurred by Li diffusion through the "shell" into the SnO_2 fiber, and natural void space facilitated the expansion of

SnO_2 upon lithiation. This unique structure effectively prevented the aggregation and pulverization of SnO_2 fibers. As the anode for LIBs, the SnO_2 fibers/rGO composites showed a superior electrochemical performance, including high Li-storage capacity and good cycling stability. The 2%-SnO_2 fibers/rGO composite possessed a discharge capacity of 1,982 mAh g^{-1} after 50 cycles at a current density of 0.4 A g^{-1}. After 1,000 cycles at a current density of 4 A g^{-1}, the composite still had a high discharge capacity of 658 mAh g^{-1}, and the capacity was restored when the current density decreased. The synthetic route presented in this work can be easily extended to the preparation of other metal or nonmetal oxides/rGO composites, such as SiO_2 and Fe_2O_3.

ACKNOWLEDGMENTS
This work was supported by National Natural Science Foundation of China (Grant No. 51662029, 21365013 and 21363015).

References

1. B.Zhao , Y.T.Xu , S.Y.Huang, K.Zhang , M. F.Yuen Matthew, J.B.Xu, X.Z.Fu , R.Sun and C.P.Wong, *Electrochim. Acta*, 202 (2016) 186.
2. L.L.Fan , X.F.Li, B.Yan , X.J.Li, D.B.Xiong , D.J.Li , H.Xu , X.F.Zhang and X.L.Sun, *Appl. Energy*, 175 (2016) 529.
3. J.H.Kong , Z.L.Liu, Z.C.Yang, H.R.Tan, S.X.Xiong, S.Y.Wong, X. Li and X.H.Lu , *Nanoscale*, 4 (2012) 525.
4. M.Xie, X.Sun , M.George , C.G.Zhou , J.Lian and Y.Zhou, *ACS Appl. Mater. Interfaces*, 7(2015) 27735.
5. K. B. Ryul, O. S. Tag and A.H. Jin, Mater. Lett., 178 (2016) 288.
6. C.L.Hsieh, D.S.Tsaig, W.W.Chiang and Y.H. Liu , *Electrochim. Acta*, 209 (2016) 332.
7. C.M.Zhang, L. Li, J.Ju and W.Chen, *Electrochim. Acta, 2*10 (2016) 181.
8. Z.F.Li, O.Liu, Y.D.Liu , F.Yang, L.Xin, Y.Zhou, H.Y.Zhang, L. Stanciu and J.Xie, *ACS Appl. Mater. Interfaces*, 7 (2015) 27087.
9. L.Luo, W.Z.Xu , Z.K.Xia, Y.Q.Fei, J.D.Zhu , C.Chen, Y.Lu, Q.F.Wei, H.Qiao and X.W.Zhang, *Ceram. Int.*, 42 (2016) 10826.
10. J.K.Wang, S.M.Xie , D.X.Cao , X.Lu, L.J.Meng, G.D.Yang and H.K.Wang, *J. Nanopart. Res.*, 18 (2016) 280.
11. Y.K.Wang, H.Y.Zhang, R..Z.Hu, J.W.Liu, V. R. Teunis, H.H.Wang, L.C.Yang and M.Zhu , *J. Alloy. Compd.*, 693(2017) 1174.
12. K. S. Hilal, A. A. Osman and A. Hatem , *Int. J. Hydrogen Energy*, 39 (2014) 21435.
13. L. A.Ma , Z. H.Wei and T. L.Guo, *J. Mater. Sci.-Mater. Electron.*, 27 (2016) 9044.
14. Y.T.Qu , Y.Z Gao, L.Wang, J.C.Rao and G.P.Yin, *Chem.-Eur. J.*, 22 (2016) 193.
15. J. Wei, T.Zeng, L. Liu, J.T. Deng, G. Zheng, P.Zhang, Y.Jin, Z.F. Jiao and X.S. Sun, *Mater. Lett.*, 180 (2016) 38.
16. J.S.Jang, S.J.Choi , S.J.Kim, M.Hakim and I.D.Kim, *Adv. Funct. Mater.*, 26 (2016) 4740.
17. X.X.Fan, X.L.He , J.P.Li, X.G.Gao and J.Jia,*Vacuum, 1*28 (2016) 112.
18. J.D.Yang, S.R.Wang, R.Dong, L.P.Zhang, Z.Y.Zhu and X.L.Gao, *Mater. Lett.*, 184 (2016) 9.
19. Z.Qiang , S. Y.Ma , H. Y.Jiao , T. T.Wang, X. H.Jiang, W. X. Jin, H. M. Yang and H. Chen, *Ceram. Int.*, 42 (2016) 18983.
20. H.Yang, Z.H.Hou, N.B.Zhou,B.H. He , J.G.Cao and Y.F.Kuang , *Ceram. Int.*, 40 (2014) 13903.
21. J.Zhu , G.H.Zhang, S.Z.Gu and B.G. Lu, *Electrochim. Acta*, 150 (2014) 308.

22. X.L.Li ,Y.L.Zhang, T.T.Li,Q.N.Zhong, H.Y. Li and J.M.Huang, *Electrochim. Acta, 1*47 (2014) 40.
23. H.M.Zhou , Z.Y.Li , Y.P.Qiu and X.Xia , *J. Alloy. Compd.*, 670 (2016) 35.
24. D. Mahmut, Y.Meltem, K.Fu, Y.Lu , H.Y.Kizil and X.W.Zhang, *J. Power Sources*, 264 (2014) 240.
25. K.Kyungil, K. Obum and P.H. Wook, *Compos. Sci. Technol.*, 133 (2016) 60.
26. Q.Yang , J.C.Zhao, T.Sun and J.Y.Yu , *Ceram. Int.*, 41 (2015) 11213.
27. K.Luo , J.H.Li , Y.L.He, L.F.Li , X.Liu , X.K.Yang and J.Y.Li , *Fuller Nanotub Car N*, 24 (2016) 531.
28. F.Xiang , M.Rahul, J.Zhong, Y.Xia , N.Y.Gu Z.Y.Yang, and K. Nikhil, *Energy Storage Materials*, 1 (2015) 9.
29. S.Y.Kong , K.Cheng, T.Ouyang, Y.Y.Gao, K.Ye, G.L.Wang and D.X.Cao, *Electrochim. Acta*, 226 (2017) 29.
30. P.Jagabandhu, H.C.Chen , C.H.Yang, C.T.Hsieh, C.Y.Su and J.K.Chang ,*Nano Energy*, 28 (2016) 124.
31. Y.Zhu, J.C.Zhang , J.Zhai and L.Jiang, *Thin Solid Films*, 510 (2006) 271.
32. B. Vahid and M. Majid, *Colloids Surf. A*, 506 (2016) 507.
33. H.Liu, B.H.Liu and Z.P.Li , *Solid State Ionics*, 294 (2016) 6.
34. Y.K.Wang , J.Ding, Y.H.Liu,Y.S. Liu , Q.Cai and J.M.Zhang, *Ceram. Int.*, 41 (2015) 15145.
35. R.X.Shen , Y.Z.Hong, J. J.Stankovich , Z.Y.Wang , S. Dai and X.B. Jin, *J. Mater. Chem. A*, 3 (2015) 17635.
36. H.T.Chen ,X.M. Pu , M.Gu , J.Zhu and L.W.Cheng , *Ceram. Int.*, 42 (2016) 17717.
37. J.Zhu and D.Deng, *Chem. Eng. Sci.*, 154 (2016) 54.
38. J.Y.Yu , T.Sun, Q.Yang and J.X.Ma, *Mater. Lett.*, 184 (2016) 169.
39. S.M.Hwang , Y.G.Lim,J.G. Kim , Y.U.Heo , J.H. Lim , Y.Yamauchi , M.S.Park, Y.J.Kim, S.X. Dou and J.H.Kim , *Nano Energy*, 10 (2014) 53.
40. Y.Li , Y.Zhao, C.L.Ma and Y.X.Kong Zhao, *Electrochim. Acta*, 218 (2016) 191.

© 2018 The Authors. Published by ESG (www.electrochemsci.org). This article is an open access article distributed under the terms and conditions of the Creative Commons Attribution license (http://creativecommons.org/licenses/by/4.0/).